$^{8}B+^{27}Al$ scattering at low energies

V. Morcelle, R. Lichtenthäler, A. Lépine-Szily, V. Guimarães, K. C. C. Pires, J. Lubian, D. R. Mendes Junior, P. N. de Faria, J. J. Kolata, F. D. Becchetti, H. Jiang, E. F. Aguilera, D. Lizcano, E. Martinez-Quiroz, and H. Garcia

The ^{8}B+^{27}Al scattering at low energies.

V. Morcelle,[1, *] R. Lichtenthäler,[2] A. Lépine-Szily,[2] V. Guimarães,[2] K.C.C. Pires,[2]

J. Lubian,[3] D.R. Mendes Junior,[3] P.N. de Faria,[3] J. J. Kolata,[4] F. D. Becchetti,[5]

H. Jiang,[5] E. F. Aguilera,[6] D. Lizcano,[6] E. Martinez-Quiroz,[6] and H. Garcia[6]

[1] *Departamento de Física, Universidade Federal Rural do Rio de Janeiro, 23851-970, Rio de Janeiro, Brazil.*
[2] *Departamento de Física Nuclear, Universidade de São Paulo, 05508-090, São Paulo, Brazil.*
[3] *Instituto de Física, Universidade Federal Fluminense,24210-340, Rio de Janeiro, Brazil.*
[4] *Department of Physics, University of Notre Dame, Notre Dame, Indiana 46556, USA.*
[5] *Department of Physics, University of Michigan, Ann Arbor, Michigan 48109-1120, USA.*
[6] *Departamento de Aceleradores, Instituto Nacional de Investigaciones Nucleares,*
Apartado Postal 18-1027, Código Postal 11801, México, Distrito Federal, México.

We present ^{8}B+^{27}Al elastic scattering angular distributions for the proton-halo nucleus ^{8}B at two energies above the Coulomb barrier, namely $E_{lab} = 15.3$ MeV and 21.7 MeV. The experiments have been performed in the Radioactive Ion Beams in Brasil facility (RIBRAS) in São Paulo, and in the *TwinSol* facility at the University of Notre Dame, USA. The angular distributions were measured in the angular range of 15-80 degrees. Optical model and Continuum Discretized Coupled Channels calculations have been performed and the total reaction cross sections have been derived. A comparison of the ^{8}B+^{27}Al total reaction cross sections with similar systems including exotic, weakly and tightly bound projectiles impinging on the same target is presented.

PACS numbers: 25.70.Bc, 25.70.Mn, 25.60.-t

I. INTRODUCTION

The scattering of nuclei away from the nuclear stability line has been one of the principal fields of research in low-energy nuclear physics over the last decades [1–8]. As one moves away from the valley of stability we find the so-called exotic nuclei which often have several interesting properties. In particular the light exotic nuclei present unusual features. Such nuclei are unstable by beta emission or electron capture, with relatively long lifetimes (milliseconds up to seconds), sufficient to produce a secondary beam. Light exotic nuclei usually present a pronounced cluster structure, with very low separation energies in comparison to their stable partners and can be found either in the neutron rich [9–18] or in the proton rich sides [19–24] of the nuclear chart. One of these nuclei is ^{8}B which is formed by a ^{7}Be core plus one proton bound by only 0.137 MeV to the core. The ^{8}B nucleus has several interesting properties. Due to its very low binding energy, it is one of the few candidates to present a proton halo on the proton rich side of the chart of nuclides. In addition, it has importance in astrophysics, particularly in the Solar model where it plays a role in the production of high energy solar neutrinos. Moreover, studies involving A=8 nuclei are relevant because of the mass gaps at A=5 and A=8. The lack of stable A=5,8 nuclei is a barrier to the nucleosynthesis of heavier elements. The doublet of mirror nuclei ^{8}Li ($T_{1/2} = 839.9ms$) and ^{8}B ($T_{1/2} = 770ms$) is unstable by beta emission and both decay to ^{8}Be which immediately decays into two alpha particles. However, due to the their relatively long life-

times, the presence of A=8 nuclei in certain astrophysical sites could provide paths for the nucleosynthesis to proceed further to the formation of heavier elements.

Because of the relevance of ^{8}B in astrophysics [25], as well as in nuclear structure and reaction theories, there are various reports in the literature studying its properties and the respective influence on different reaction mechanisms [26–37]. These works report experimental data and/or theoretical calculations for the elastic, breakup and fusion cross sections.

Scattering data involving $A = 8$ nuclei are scarce (especially data involving light targets) yet important because they can provide information about the nuclear interaction potential which is a necessary ingredient in many calculations of astrophysical interest.

To contribute to the study of reactions involving ^{8}B nucleus we present here ^{8}B+^{27}Al scattering measurements at or near Coulomb barrier energies, where the interplay of different reaction mechanisms is expected to be more intensive. These results complement those in a previous publication on ^{7}Be scattering [24] which is the core of ^{8}B.

In section II we describe the experiment, in section III we present the results of optical model and a Continuum Discretized Coupled Channels (CDCC) analysis. In section IV we present a comparison of the total reaction cross section derived in the present work from the elastic scattering of ^{8}B+^{27}Al system with the ones of several other weakly and tightly bound systems. Finally in section V we present some conclusions.

II. EXPERIMENT

The measurements have been carried out in two experiments performed at the Nuclear Physics Open Labora-

* vivianemorcelle@gmail.com

tory (LAFN) of the University of São Paulo, Brazil and at the Nuclear Structure Laboratory (NSL) of the University of Notre Dame, USA. In both experiments the ^{8}B secondary beam was produced by the ^{3}He(^{6}Li,^{8}B) reaction using a ^{6}Li primary beam and a ^{3}He gas target. The energies of the ^{6}Li primary beams were 26.5 and 32.6 MeV, respectively, in the RIBRAS and *TwinSol* facilities.

In the RIBRAS facility the primary target consisted of a 3.6 cm length gas cell filled with 1 atm of ^{3}He gas, held by two 2.2μm havar windows. The primary target was bombarded with a 26.5 MeV ^{6}Li^{3+} beam of intensity around 300 nAe, producing a mixture of ^{8}B, ^{7}Be, ^{6}Li, and α particles. The intensity of the ^{8}B beam was of about 10^4 particles per second. The ^{8}B beam was focused by the first RIBRAS solenoid into a scattering chamber located between the two solenoids where the secondary targets and detectors had been mounted. The detection system consisted of one silicon $\Delta E(20\mu m)$-E(1000μm) telescope placed at forward angles and two single E(1000μm) detectors at backward angles. The telescope was mounted in the forward angles where the secondary beam particles had sufficient energy to cross through the 20μm ΔE detector, allowing particle identification. The single E detectors were used at backward angles where the scattered ^{8}B peak is well separated in energy from the other contaminant beams. An example of measured two dimensional and single spectra are shown in Figures 1 and 2, respectively.

Two secondary targets have been used, ^{27}Al of 2.1 mg/cm^2 and ^{197}Au of 4.6 mg/cm^2. The latter was used for normalization purposes, since the scattering on gold is pure Rutherford at these energies.
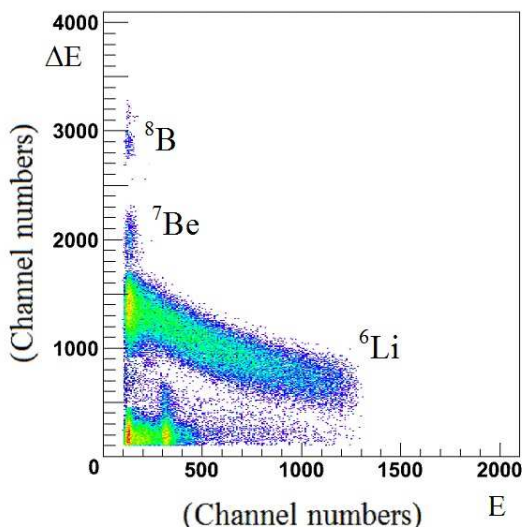
formed in the 10 MV tandem of the Nuclear Structure Laboratory of the University at Notre Dame, with the *TwinSol* system. The ^{8}B production reaction and primary target setup was the same as in the RIBRAS experiment. Two solenoids were used to select the secondary beam with no absorber in the mid-plane. The ^{8}B beam intensity was of the order of 10^4 pps for a ^{6}Li beam intensity of 350 nAe. The detection setup consisted of four (x-y) position-sensitive detectors (PSD) of $23 \times 23 mm$ to cover the angular range from $20-55$ deg in the laboratory frame. A single $\Delta E - E$ telescope was placed at 15 deg to provide particle identification. The analysis of these data was performed by dividing the PSD detectors (x-signal) into two halfs (due to the low statistics), so as only two angles per detector were obtained. A blocker was placed on the forward half of the more frontal PSD detector to avoid direct beam on it. The absolute normalization of the cross sections was provided by normalization measurements using a gold target.

The ^{8}B+^{27}Al angular distributions are presented in Figure 3. An important point to consider in this experiment concerns the energy loss in the secondary targets. The targets are thick and the ^{8}B loses a considerable amount of its initial energy during its path through the target. As a consequence, the measured cross section is the result of an energy average over the target thickness. In reference [24] we have shown that, for pure Rutherford scattering, the energy average is equivalent to the cross section at a certain equivalent energy given by E$_{eq}$= $\sqrt{E_0 E_1}$ where E$_0$ and E$_1$ are the beam energies respectively before and after the target. As our measurements have been performed at energies around the Coulomb barrier, where the Rutherford scattering dominates, we adopt the geometrical mean as the nominal energy of the angular distributions. Thus we will refer to E$_0$ for the incident ^{8}B energy before the target and to E$_{eq}$, as defined above, for the energy of the angular distributions. The Coulomb barrier for this system is at $V_B^{lab} = 13.42$ MeV using the formula deduced in Ref. [38].

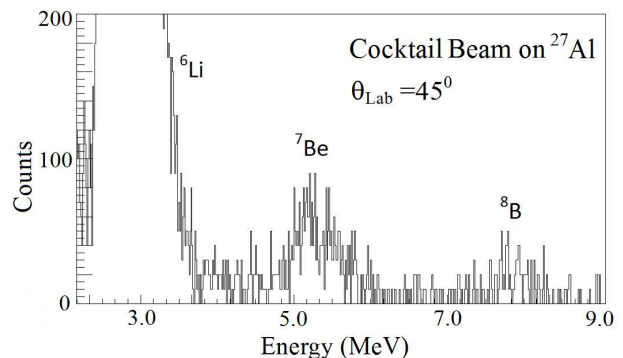Figure 1. (color online) Bidimensional $\Delta E - E$ spectrum for ^{8}B+^{27}Al corresponding to an average energy E$_{eq}$ =15.3 MeV and $\theta_{lab} = 20^0$.

Figure 2. One dimensional spectrum for the secondary beam scattered on ^{27}Al obtained at the RIBRAS facility. The ^{8}B beam incident energy is E$_0$=18.0 MeV.
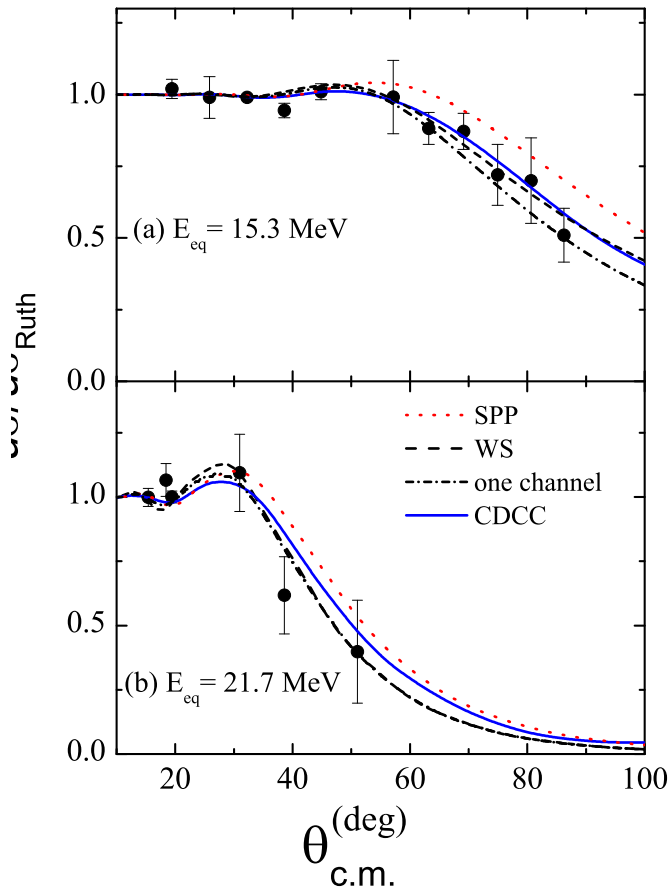
The experiment at the higher energy has been per-

Figure 3. (color online) The ^{8}B $+^{27}$Al elastic scattering angular distributions. The solid circles represent the experimental data, while the dotted red and the dashed curves are the results of calculations using the SPP and WS potential, respectively. The CDCC results are represented by the solid blue curve and the dot-dashed curves represents results where all the couplings are switched off (one-channel).

III. THEORETICAL ANALYSIS

A. Optical Model Analysis

The elastic scattering angular distributions have been analyzed by optical model (OM) and Continuuum Discretized Coupled Channels Calculations (CDCC).

We performed optical model calculations using two different types of nuclear potentials, the usual São Paulo Potential (SPP) [39] and a Woods-Saxon (WS) potential described below [38]. At near barrier energies, the São Paulo potential is essentially an usual double folding potential that has no free parameters, since it has been derived from the systematics of nuclear matter densities in the region. It has been recently shown [34] that mi-

Table I. Values of energy and the strengths of the real and imaginary parts of the WS potential (in MeV) and the calculated total reaction cross sections (in mb).

E_0	E_{eq}^{lab}	V_0	W_0	σ_R	χ^2/N	setup
18.0	15.3	21.7	29.6	506	0.31	RIBRAS
24.1	21.7	32.1	16.0	1074	0.99	TwinSol

croscopic Hartree Fock Bogolyubov calculations for the matter densities of ^{8}B nucleus give very similar results for the cross section of the ^{8}B $+ ^{58}$Ni system when compared with ones obtained using the matter density from systematics. The São Paulo potential was used for the real and imaginary parts of the optical potential with strength coefficients $N_r = 1$ and $N_I = 0.78$, respectively. The results of these calculations are shown in Figure 3 as the dotted curves. The total reaction cross sections obtained from the São Paulo potential calculations are: 351.8 mb at 15.3 MeV and 895.0 mb at 21.7 MeV.

For the Woods-Saxon we used a potential introduced in Ref. [38]:

$$V_n(r) = -V_0 f(r, R_v, a_v) - iW_0 f(r, R_w, a_w), \quad (1)$$

where the Woods-Saxon form factor is given by:

$$f(r, R_i, a_i) = \frac{1}{1 + \exp \frac{r - R_i}{a_i}}; i = v, w \quad (2)$$

where V_0 and W_0 represent depths of the real and imaginary parts of the potential, respectively. The radii are given by $R_i = r_{0i}(A_p^{1/3} + A_t^{1/3})$ where r_{0i} are the reduced radii and a_i the diffusenesses. The index p, t stands for the projectile and the target, respectively.

This potential has a fixed geometry $r_{0v} = r_{0w} = 1.3$ fm and $a_v = a_w = 0.65$ fm and, the depths V_0 and W_0 are varied to fit the data [38]. In reference [38] it has been shown that a Woods-Saxon form factor with this geometry and depths between $10 - 20$ MeV can reproduce quite well the tail of the double folding potential for a number of stable systems. We used the same procedure here and obtained again good agreement between the Woods-Saxon and double folding potentials in the tail region, the important region for the description of the elastic scattering.

All calculations were performed using the code SFRESCO [40], the search version of the FRESCO code. The final results are shown as dashed curves in Figure 3. The agreement with the experimental data is very good, as expected from a fitting procedure. In Table I the final parameters V_0 and W_0, the total reaction cross sections obtained and the χ^2/N, that refers to the χ^2 per experimental point, are presented.

B. CDCC Analysis

It is well known that the best technique to study the elastic breakup is the CDCC method [41–43]. By elastic breakup it is understood a process where after the breakup all the fragments of the broken nucleus remain in its intrinsic ground state, as well as the target nucleus that participates in the reaction. The potential energy of the interaction is transformed to relative kinetic energy of the fragments that feed different continuum states. The effect of target excitations and other possible reaction mechanisms are taken into account through the effective optical potential of the interactions of the fragments and the target (if one supposes that the projectile is the nucleus that breaks during the interaction). CDCC calculations involving the ^{8}B proton-halo projectile have been reported for different targets ranging from the light ^{12}C [26], medium mass ^{58}Ni [27–30] and heavy ^{208}Pb [31, 32] targets. Most of the studies have been concentrated on the elastic, quasi elastic, or breakup cross section.

Our present CDCC calculations used the same model space as in previous papers [26–30]. The ^{8}B projectile is modelled as an inert core of ^{7}Be plus a proton as a valence particle. Its ground state wave function is a $1p_{3/2}$ state bound by 0.137 MeV. The binning method was used to generate a basis on which the total wave function can be expanded and has a property of being square-integrable wave functions. They are obtained by averaging, in some energy interval, the scattering wave function of the relative motion of the proton and the core [41]. The bin state discretization was carried out up to maximum relative energy $\varepsilon_{max} = 8$ MeV, equally spaced in momentum. The continuum bins were calculated integrating up to $R_{bin} = 60$ fm. This distance was enough to guarantee the orthogonality between bin wave functions. Bins with relative p-^{7}Be orbital angular momenta $l \leqslant 3$ were included. The optical potential to derive the p-^{7}Be wave functions was taken from [44]. The real part of this potential was also used to bind the ^{8}B ground state. As all interactions are independent of the ^{7}Be intrinsic spin, it was neglected.

Concerning the projectile-target relative movement, the convergence was obtained by using partial waves up to $L_{\max} = 1000$ and radii up to $R_{max} = 500$ fm for the computation of the relative-motion wave functions. In the expansion of the projectile-target potential multipoles up to $\lambda \leqslant 3$ were considered. For both proton – ^{27}Al and ^{7}Be – ^{27}Al optical potentials the standard São Paulo potential [39] was used for both real and imaginary parts with strength coefficients $N_R = 1.0$ and $N_I = 0.78$, respectively. This prescription has been shown to be successful for describing the elastic scattering of many systems in a wide energy interval [45]. The calculations were performed using FRESCO code [40].

The results of CDCC calculations, represented by the solid curve, are compared with the experimental elastic scattering angular distributions in figure 3. From this figure one can see a very good agreement with the experimental data. The total reaction cross sections from these calculations are of 566.4 mb and 1141.4 mb respectively for 15.3 MeV and 21.7 MeV energies. The results of the reaction cross section derived from these calculations are in reasonable agreement with the ones shown in Table I for the case of Woods-Saxon potential fit, especially having in mind that the CDCC calculations are not fitting experimental results but instead, predictions.

In figure 3, we also show the results of the calculations where all the continuum couplings are switched off (described as one channel in the legend of figure 3) and shown as the dotted-dashed curve.

The comparison of the one-channel and the full CDCC calculations shows that, although the effect of the breakup channel is not strong, this channel has a non negligible effect on the elastic scattering angular distribution. It is also observed that the breakup channel slightly damps the so called Coulomb rainbow peak and increases the cross section at angles larger than the rainbow peak. The same qualitative effect has been recently observed in ^{6}He+^{58}Ni [15], ^{11}Li + ^{208}Pb [17] and ^{11}Be + ^{64}Zn [18] scattering. It also has been shown [32] that the damping of the Coulomb rainbow peak for the ^{8}B + ^{208}Pb, ^{58}Ni systems involving proton-halo projectiles is smaller than for the systems involving neutron-halo projectiles (like ^{11}Li and ^{6}He) because the dipole response of the ^{8}B is less. As in the present study where the charge of the target is smaller, an almost negligible effect was expected. It was also shown in Ref. [32] that the enhancement of the elastic angular distribution at backward angles is mainly due to the quadrupole interactions.

Although for the CDCC calculations the São Paulo potential was also used, the results differ from the ones represented as a dotted curve. The reason for this disagreement lies in the fact that the so-called one channel results are OM calculations using the optical potential that is a single folding of the p-target plus ^{7}Be-target interaction by a ground state wave function of the projectile (φ_0),

$$V_{00} = \left\langle \varphi_0 \left| V_{p-^{27}Al} + V_{^7Be-^{27}Al} \right| \varphi_0 \right\rangle. \qquad (3)$$

The potential of the expression 3 takes into account explicitly the halo structure of the ^{8}B projectile, while the optical potential of the calculations used in the previous section did not.

IV. TOTAL REACTION CROSS SECTION

In addition to the nuclear interacting potential, Optical Model and CDCC calculations also provide the total reaction cross sections. In order to compare total reaction cross sections between different systems one has to reduce the cross sections to remove trivial effects due to the different sizes and different Coulomb barriers. Several methods have been proposed to reduce total reac-

tion cross sections [46–48] and here, as a first step, we simply divide the cross sections by πR_b^2 and the C.M. energies by V_b, where R_b is the position of the Coulomb barrier and V_b is its height. Both R_b and V_b have been calculated using the formula presented in [38], which provide Coulomb barrier positions and heights in very good agreement with those obtained using numerical double folding nuclear potential calculations.

The OM and CDCC ^{8}B+^{27}Al total reaction cross sections obtained in this work have been averaged and reduced to compare with other systems with different projectiles, all on ^{27}Al target. The experimental data were taken from Ref. [49] for the ^{16}O + ^{27}Al system, from Ref. [50] for the ^{6}He + ^{27}Al system, from Ref. [51] for the ^{7}Li + ^{27}Al system, from Ref. [52] for the ^{6}Li + ^{27}Al system, from Refs. [53, 54] for the ^{9}Be + ^{27}Al system and from Ref. [24] for the ^{7}Be + ^{27}Al system.

The results are presented in Figure 4. As the Coulomb barrier parameters V_b and R_b used in the reduction procedure are realistic, the obtained reduced cross sections and energies exhibit a direct relation to the geometric cross sections and realistic Coulomb barrier energies. We see that the weakly bound and exotic systems all present larger reduced cross sections compared to the stable double magic projectile ^{16}O.
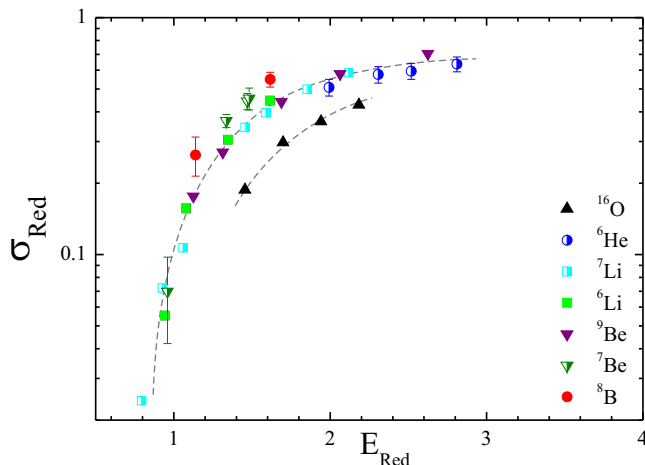

Figure 4. (color online) Reduced reaction cross sections for several projectiles on ^{27}Al target. The dashed curves are a guide to the eyes.

One step further in the present analysis would be to try to disentangle the effect of the breakup channel on the total reaction cross section. For this purpose we calculate a reaction cross section, which includes the effect of the most important reaction channels, other than breakup, and rescale the experimental total reaction cross section by this quantity. At near barrier energies and for light systems the principal reaction channels contributing to the total reaction cross section are: the total fusion (σ_{TF}), the inelastic excitations of the target and/or the projectile (σ_{inel}), particle transfer (σ_{tr}), and the breakup cross section (σ_{BU}), if weakly bound nuclei are involved,

$$\sigma_R = \sigma_{TF} + \sigma_{inel} + \sigma_{BU} + \sigma_{tr}. \qquad (4)$$

The effect of inelastic excitations is taken into acount by coupled channel calculations including the five low lying states of ^{27}Al: $1/2^+$, $3/2^+$, $7/2^+$, $5/2^+$ and $9/2^+$. These states are effectively treated as a single state as a $1d_{5/2}$ proton hole coupled to the first 2^+ state of the ^{28}Si core. The quadrupole deformation parameter of ^{28}Si was taken from Ref. [55].

The São Paulo potential [39] was used for the real part of the optical potential and for the imaginary part, a Woods-Saxon form-factor with parameters $W_0 = 50$ MeV, $r_w = 1.06$ fm and $a_w = 0.2$ fm for the depth, reduced radius and diffuseness was used. As we are using a potential with matter density systematics, all the systems will be treated with the same conditions. The imaginary potential internal to the Coulomb barrier like this is equivalent to the so called ingoing-wave boundary conditions that yields the absorption of the flux that is passed through or over the Coulomb barrier. This imaginary potential accounts for the total fusion. It has been proved that although the complete fusion is hindered at energies above the barrier (for the heavy systems involving weakly bound nuclei), the experimental total fusion data coincides with the results of coupled channel cross sections derived without taking into account the breakup channel [7] (and references therein). So, the results of our coupled channel calculations for the the total reaction cross sections correspond to the sum of $\sigma_{TF} + \sigma_{inel}(^{27}$Al). If there were no other important reaction channels the ratio of the experimental (σ^{exp}) to the coupled channel (σ^{CC}) total reaction cross section will be equal to 1.0. The existence of other reaction channels will produce values of the ratio $\sigma^{exp}/\sigma^{CC} \geqslant 1.0$.

We would like to emphasize that we put more attention to the results for energies above the Coulomb barrier ($E_{red} \geqslant 1$). The reason is that the major part of the data found in the literature for the total reaction cross section were derived by fitting the experimental elastic scattering angular distributions. At energies below the Coulomb barrier, the elastic cross section is almost Rutherford's and very insensitive to the nuclear potential. This lead to bigger uncertainties in the determination of the total reaction cross section.

As we are not including the transfer channels in our coupling scheme (because of the lack of the needed spectroscopic information), the reason for the reduced cross section for some systems to be bigger than that for others will be caused by the effect of transfer plus breakup channels (and by the inelastic excitation to the first excited state of ^{7}Li, not included in the coupling scheme for the ^{7}Li + ^{27}Al system).

In Figure 5 we show our results for the reduction of the experimental total reaction cross section by the coupled channel results. One can see that the lower value for the ratio σ^{exp}/σ^{CC} is in fact found for reactions induced by
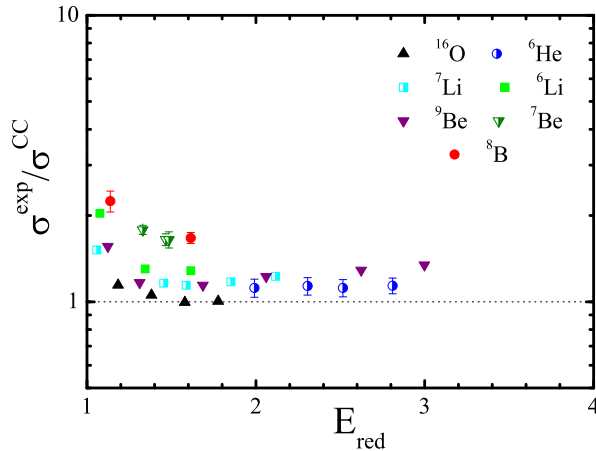
Figure 5. (color online) Comparison of reduced total reaction cross section for the same systems shown in Fig. 4 for the case of the reduction of σ^{exp} by σ^{CC}. See text for details.

the ^{16}O projectile, the only tightly bound projectile included in our study. All the other weakly bound systems have larger and about the same value of the σ^{exp}/σ^{CC} ratio. Some extra increment is observed for reactions induced by the proton-halo ^{8}B projectile. For reactions induced by a ^{8}B projectile we have only two data points located at energies just above V_b. It would be interesting to see if this behaviour remains valid for higher energies. These conclusions are in agreement with the qualitative ones shown in figure 4.

V. SUMMARY AND CONCLUSIONS

In summary, two angular distributions for the ^{8}B+^{27}Al scattering have been measured at energies above the Coulomb barrier. Optical Model and CDCC calculations have been performed. The optical model analysis was performed using the standard double folding São Paulo

Potential and, a Woods-Saxon shape with fixed geometry, varying only the depths V_0 and W_0 to fit the data. The results show that the standard São Paulo Potential overestimates the cross sections in the region where $d\sigma/d\sigma_{Ruth} < 1$. The Wood-Saxon potential, on the other hand, reproduces quite well the shape of the angular distribution.

As a second step in the analysis we performed continuum discretized coupled channel calculations to take into account the effect of the ^{8}B breakup. The calculations are in very good agreement with the data considering that there are no free parameters in this calculations. A one-channel (no coupling) CDCC calculation was performed and compared to the full CDCC result. This comparison shows that the effect of the coupling to the projectile breakup channel is to reduce the amplitude of the Fresnel peak and increase the cross section at backward angles.

The total reaction cross sections have been obtained and are compared in a reduced cross section plot with systems for other projectiles on the same target. The reactions induced by the exotic ^{8}B , ^{6}He and weakly bound ^{7,9}Be, ^{6,7}Li projectiles present a higher reduced cross section when compared to the ones induced by the tightly bound ^{16}O projectile.

A quantitative analysis of the influence of the breakup plus transfer channels was performed by explicitly including the effects of the inelastic scattering and the total fusion channels for the total reaction cross sections calculations. The results indicate that the breakup plus transfer channels have a considerable effect on the total reaction cross sections, increasing it for lower energies. These results appear to be in agreement with the ones obtained by the simpler reduction procedure.

[1] N. Keeley, N. Alamanos, K. W. Kemper, and K. Rusek, Prog. Part. Nucl. Phys., **63**, 396 (2009).
[2] N. Keeley, R. Raabe, N. Alamanos, and J. L. Sida, Prog. Part. Nucl. Phys., **59**, 579 (2007).
[3] A. Lépine-Szily, R. Lichtenthäler, and V. Guimarães, Eur. Phys. J. A, **50**, 128 (2014).
[4] R. Lichtenthäler, A. Lépine-Szily, V. Guimarães, C. Perego, V. Placco, O. Camargo Jr, R. Denke, P. N. de Faria, E. A. Benjamim, N. Added, G. F. Lima, M. S. Hussein, J. J. Kolata, and A. Arazi, Eur. Phys. J. A, **25**, 733 (2005).
[5] B. B. Back, H. Esbensen, C. L. Jiang, and K. E. Rehm, Rev. Mod. Phys., **86**, 317 (2014).
[6] L. F. Canto, P. R. S. Gomes, R. Donangelo, J. Lubian,

and M. S. Hussein, Phys. Rep., **596**, 1 (2015).
[7] P. R. S. Gomes, J. Lubian, L. F. Canto, D. R. Otomar, D. R. Mendes Junior, P. N. de Faria, R. Linares, L. Sigaud, J. Rangel, J. L. Ferreira, E. Ferioli, B. Paes, E. N. Cardozo, M. R. Cortes, M. Ermamatov, P. Lotti, and M. S. Hussein, Few-Body Systems, **57**, 165 (2016).
[8] J. J. Kolata, V. Guimarães, and E. F. Aguilera, Eur. Phys. J. A, **52**, 1 (2016).
[9] E. A. Benjamim et al., Phys. Lett. B, **647**, 30 (2007).
[10] P. N. de Faria, R. Lichtenthäler, K. C. C. Pires, A. M. Moro, A. Lépine-Szily, V. Guimarães, D. R. Mendes, A. Arazi, M. Rodríguez-Gallardo, A. Barioni, V. Morcelle, M. C. Morais, O. Camargo, J. Alcântara Nuñes, and M. Assunção, Phys. Rev. C, **81**, 044605 (2010).

[11] P. N. de Faria, R. Lichtenthäler, K. C. C. Pires, A. M. Moro, A. Lépine-Szily, V. Guimarães, D. R. Mendes, A. Arazi, A. Barioni, V. Morcelle, and M. C. Morais, Phys. Rev. C, **82**, 034602 (2010).

[12] P. Mohr, P. N. de Faria, R. Lichtenthäler, K. C. C. Pires, V. Guimarães, A. Lépine-Szily, D. R. Mendes, A. Arazi, A. Barioni, V. Morcelle, and M. C. Morais, Phys. Rev. C, **82**, 044606 (2010).

[13] K. C. C. Pires, R. Lichtenthäler, A. Lépine-Szily, V. Guimarães, P. N. de Faria, A. Barioni, D. R. Mendes Junior, V. Morcelle, R. Pampa Condori, M. C. Morais, J. C. Zamora, E. Crema, A. M. Moro, M. Rodríguez-Gallardo, M. Assunção, J. M. B. Shorto, and S. Mukherjee, Phys. Rev. C, **83**, 064603 (2011).

[14] K. C. C. Pires, R. Lichtenthäler, A. Lépine-Szily, and V. Morcelle, Phys. Rev. C, **90**, 027605 (2014).

[15] V. Morcelle, K. C. C. Pires, M. Rodríguez-Gallardo, R. Lichtenthäler, A. Lépine-Szily, V. Guimarães, P. N. Faria, D. R. Mendes Junior, A. M. Moro, L. R. Gasques, E. Leistenschneider, R. Pampa Condori, V. Scarduelli, M. C. Morais, A. Barioni, J. C. Zamora, and J. M. B. Shorto, Phys. Lett. B, **732**, 228 (2014).

[16] O. Camargo, V. Guimarães, R. Lichtenthäler, V. Scarduelli, J. J. Kolata, C. A. Bertulani, H. Amro, F. D. Becchetti, H. Jiang, E. F. Aguilera, D. Lizcano, E. Martinez-Quiroz, and H. Garcia, Phys. Rev. C, **78**, 034605 (2008).

[17] M. Cubero, J. P. Fernández-García, M. Rodríguez-Gallardo, L. Acosta, M. Alcorta, M. A. G. Alvarez, M. J. G. Borge, L. Buchmann, C. A. Diget, H. A. Falou, B. R. Fulton, H. O. U. Fynbo, D. Galaviz, J. Gómez-Camacho, R. Kanungo, J. A. Lay, M. Madurga, I. Martel, A. M. Moro, I. Mukha, T. Nilsson, A. M. Sánchez-Benítez, A. Shotter, O. Tengblad, and P. Walden, Phys. Rev. Lett., **109**, 262701 (2012).

[18] A. Di Pietro, G. Randisi, V. Scuderi, L. Acosta, F. Amorini, M. J. G. Borge, P. Figuera, M. Fisichella, L. M. Fraile, J. Gomez-Camacho, H. Jeppesen, M. Lattuada, I. Martel, M. Milin, A. Musumarra, M. Papa, M. G. Pellegriti, F. Perez-Bernal, R. Raabe, F. Rizzo, D. Santonocito, G. Scalia, O. Tengblad, D. Torresi, A. M. Vidal, D. Voulot, F. Wenander, and M. Zadro, Phys. Rev. Lett., **105**, 022701 (2010).

[19] J. Liang, J. Beene, A. Caraley, H. Esbensen, A. Galindo-Uribarri, C. Gross, P. Mueller, K. Schmitt, D. Shapira, D. Stracener, and R. Varner, Phys. Lett. B, **681**, 22 (2009).

[20] J. F. Liang, J. R. Beene, H. Esbensen, A. Galindo-Uribarri, J. Gomez del Campo, C. J. Gross, M. L. Halbert, P. E. Mueller, D. Shapira, D. W. Stracener, I. J. Thompson, and R. L. Varner, Phys. Rev. C, **65**, 051603 (2002).

[21] E. F. Aguilera, E. Martinez-Quiroz, D. Lizcano, A. Gómez-Camacho, J. J. Kolata, L. O. Lamm, V. Guimarães, R. Lichtenthäler, O. Camargo, F. D. Becchetti, H. Jiang, P. A. DeYoung, P. J. Mears, and T. L. Belyaeva, Phys. Rev. C, **79**, 021601 (2009).

[22] M. Romoli, E. Vardaci, M. Di Pietro, A. De Francesco, A. De Rosa, G. Inglima, M. La Commara, B. Martin, D. Pierroutsakou, M. Sandoli, M. Mazzocco, T. Glodariu, P. Scopel, C. Signorini, R. Bonetti, A. Guglielmetti, F. Soramel, L. Stroe, J. Greene, A. Heinz, D. Henderson, C. L. Jiang, E. F. Moore, R. C. Pardo, K. E. Rehm, A. Wuosmaa, and J. F. Liang, Phys. Rev. C, **69**, 064614 (2004).

[23] J. C. Zamora, V. Guimarães, A. Barioni, A. Lépine-Szily, R. Lichtenthäler, P. N. de Faria, D. R. Mendes, L. R. Gasques, J. M. B. Shorto, V. Scarduelli, K. C. C. Pires, V. Morcelle, E. Leistenschneider, R. P. Condori, V. A. Zagatto, M. C. Morais, and E. Crema, Phys. Rev. C, **84**, 034611 (2011).

[24] V. Morcelle, R. Lichtenthäler, R. Linares, M. C. Morais, V. Guimarães, A. Lépine-Szily, P. R. S. Gomes, J. Lubian, D. R. Mendes Junior, P. N. De Faria, A. Barioni, L. R. Gasques, J. M. B. Shorto, K. C. C. Pires, J. C. Zamora, R. P. Condori, V. Scarduelli, J. J. Kolata, H. Amro, F. D. Becchetti, H. Jiang, E. F. Aguilera, D. Lizcano, E. Martinez-Quiroz, and H. Garcia, Phys. Rev. C, **89**, 044611 (2014).

[25] E. G. Adelberger et al., Rev. Mod. Phys., **83**, 195 (2011).

[26] B. Paes, J. Lubian, P. R. S. Gomes, and V. Guimaraes, Nucl. Phys. A, **890**, 1 (2012).

[27] F. M. Nunes and I. J. Thompson, Phys. Rev. C, **59**, 2652 (1999).

[28] J. Lubian and F. M. Nunes, J. Phys. G. Nucl. Part. Phys., **34**, 513 (2007).

[29] J. Lubian, T. Correa, P. Gomes, and L. F. Canto, Phys. Rev. C, **78**, 064615 (2008).

[30] J. Lubian, T. Correa, E. F. Aguilera, L. F. Canto, A. Gomez-Camacho, E. M. Quiroz, and P. R. S. Gomes, Phys. Rev. C., **79**, 064605 (2009).

[31] Y. Y. Yang, J. S. Wang, Q. Wang, D. Pang, J. B. Ma, M. R. Huang, J. L. Han, P. Ma, S. L. Jin, Z. Bai, Q. Hu, L. Jin, J. B. Chen, N. Keeley, K. Rusek, R. Wada, S. Mukherjee, Z. Y. Sun, R. F. Chen, X. Y. Zhang, Z. G. Hu, X. H. Yuan, X. G. Cao, Z. G. Xu, S. W. Xu, C. Zhen, Z. Q. Chen, Z. Chen, S. Z. Chen, C. M. Du, L. M. Duan, F. Fu, B. X. Gou, J. Hu, J. J. He, X. G. Lei, S. L. Li, Y. Li, Q. Y. Lin, L. X. Liu, F. D. Shi, S. W. Tang, G. Xu, X. Xu, L. Y. Zhang, X. H. Zhang, W. Zhang, M. H. Zhao, Z. Y. Guo, Y. H. Zhang, H. S. Xu, and G. Q. Xiao, Phys. Rev. C, **87**, 044613 (2013).

[32] J. Rangel, J. Lubian, L. F. Canto, and P. R. S. Gomes, Phys. Rev. C, **93**, 054610 (2016).

[33] J. A. Tostevin, F. M. Nunes, and I. J. Thompson, Phys. Rev. C, **63**, 024617 (2001).

[34] J. Rangel, J. Lubian, P. R. S. Gomes, B. V. Carlson, L. C. Chamon, and A. Gomez Camacho, Eur. Phys. J. A, **49**, 57 (2013).

[35] E. F. Aguilera, P. Amador-Valenzuela, E. Martinez-Quiroz, D. Lizcano, P. Rosales, H. García-Martínez, A. Gómez-Camacho, J. J. Kolata, A. Roberts, L. O. Lamm, G. Rogachev, V. Guimarães, F. D. Becchetti, A. Villano, M. Ojaruega, M. Febbraro, Y. Chen, H. Jiang, P. A. DeYoung, G. F. Peaslee, C. Guess, U. Khadka, J. Brown, J. D. Hinnefeld, L. Acosta, E. S. Rossi Jr, J. F. P. Huiza, and T. L. Belyaeva, Phys. Rev. Lett., **107**, 092701 (2011).

[36] A. Gomez Camacho, E. F. Aguilera, J. Lubian, and P. R. S. Gomes, J. Phys. G: Nucl. Part. Phys., **40**, 035103 (2013).

[37] A. Pakou, E. Stiliaris, D. Pierroutsakou, N. Alamanos, A. Boiano, C. Boiano, D. Filipescu, T. Glodariu, J. Grebosz, A. Guglielmetti, M. La Commara, M. Mazzocco, C. Parascandolo, K. Rusek, A. M. Sánchez-Benítez, C. Signorini, O. Sgouros, F. Soramel, V. Soukeras, E. Strano, L. Stroe, N. Toniolo, D. Torresi, and K. Zerva, Phys. Rev. C, **87**, 014619 (2013).

[38] A. S. Freitas, L. Marques, X. X. Zhang, M. A. Luzio,

P. Guillaumon, R. P. Condori, and R. Lichtenthäler, Braz. J. Phys., **46**, 120 (2016).

[39] L. C. Chamon, B. V. Carlson, L. R. Gasques, D. Pereira, C. De Conti, M. A. G. Alvarez, M. S. Hussein, M. A. Cândido Ribeiro, E. S. Rossi Jr, and C. P. Silva, Phys. Rev. C, **66**, 014610 (2002).

[40] I. Thompson, Comp. Phys. Rep., **7**, 167 (1988).

[41] Y. Sakuragi, M. Yahiro, and M. Kamimura, Prog. Theor. Phys. Suppl., **89**, 136 (1986).

[42] G. H. Rawitscher, Phys. Rev. C, **9**, 2210 (1974).

[43] G. H. Rawitscher, Nucl. Phys. A, **241**, 365 (1975).

[44] H. Esbensen and G. F. Bertch, Nucl. Phys. A, **60**, 37 (1996).

[45] L. R. Gasques, L. C. Chamon, P. R. S. Gomes, and J. Lubian, Nucl. Phys. A, **764**, 135 (2006).

[46] P. R. S. Gomes, J. Lubian, I. Padrón, and R. M. Anjos, Phys. Rev. C, **71**, 017601 (2005).

[47] L. F. Canto, D. R. Mendes Junior, P. R. S. Gomes, and J. Lubian, Phys. Rev. C, **92**, 014626 (2015).

[48] P. R. S. Gomes, D. R. Mendes Junior, L. F. Canto, J. Lubian, and P. N. de Faria, Few Body Syst., **57**, 205 (2016).

[49] E. Crema, Masters degree thesis, Universidade de São Paulo (1979), unpublished.

[50] E. A. Benjamim, A. Lépine-Szily, D. R. M. Junior, R. Lichtenthäler, V. G. aes, P. R. S. Gomes, L. C. Cha-mon, M. S. Hussein, A. M. Moro, A. Arazi, I. Padrón, J. A. N. nez, M. A. ao, A. Barioni, O. C. Jr, R. Z. Denke, P. N. de Faria, and K. C. C. Pires, Phys. Lett.B, **647**, 30 (2007).

[51] J. M. Figueira, D. Abriola, J. O. Fernández Niello, A. Arazi, O. A. Capurro, E. d. Barbará, G. V. Martí, D. Martínez Heimann, A. J. Pacheco, J. E. Testoni, I. Padrón, P. R. S. Gomes, and J. Lubian, Phys. Rev. C, **73**, 054603 (2006).

[52] J. M. Figueira, J. O. Fernández Niello, D. Abriola, A. Arazi, O. A. Capurro, E. de Barbará, D. Martínez Heimann, A. E. Negri, A. J. Pacheco, I. Padrón, P. R. S. Gomes, J. Lubian, T. Correa, and B. Paes, Phys. Rev. C, **75**, 017602 (2007).

[53] P. R. S. Gomes, R. M. Anjos, C. Muri, J. Lubian, I. Padrón, L. C. Chamon, R. Liguori Neto, N. Added, J. O. Fernández Niello, G. V. Martí, O. A. Capurro, A. J. Pacheco, J. E. Testoni, and D. Abriola, Phys. Rev., **C70**, 054605 (2004).

[54] G. V. Martí, P. R. S. Gomes, M. D. Rodriguez, J. O. Fernández Niello, O. A. Capurro, A. J. Pacheco, J. E. Testoni, M. Ramirez, A. Arazi, I. Padrón, R. M. Anjos, J. Lubian, and E. Crema, Phys. Rev.C, **71**, 027602 (2005).

[55] S. Raman, C. Nestor, Jr., and P. Tikkanen, Atomic Data and Nuclear Data Tables, **78**, 1 (2001).